nature climate change

LETTERS

PUBLISHED ONLINE: 9 MARCH 2014 | DOI: 10.1038/NCLIMATE2142

Fewer large waves projected for eastern Australia due to decreasing storminess

Andrew J. Dowdy*, Graham A. Mills, Bertrand Timbal and Yang Wang

Extratropical cyclones are the main generators of the strong winds that cause large ocean waves in temperate regions of the world. The severity of the winds associated with these storms is poorly represented by the coarse resolution of current global climate models (GCMs), making it challenging to produce projections of the future climate of large waves. Wind data from GCMs can be downscaled in resolution using dynamical methods, resulting in a successful reproduction of the mean wave climate, but a suboptimal reproduction of the storm wave climate[1]. Projections of large wave occurrence can also be produced using statistical downscaling methods, although such methods have previously been applied only to three or less GCMs[2,3], preventing a robust assessment of confidence in projections based on variation between models. Consequently, considerable uncertainty remains in projections of the future storm wave climate. Here we apply a statistical diagnostic of large wave occurrence in eastern Australia to 18 different GCMs, allowing model variations to be examined in greater detail than previously possible. Results are remarkably consistent between different GCMs, allowing anthropogenic influences to be clearly demonstrated, with fewer days with large waves expected to occur in eastern Australia due to increasing greenhouse gas concentrations.

There is growing interest in understanding the climatology of surface ocean waves, partly due to their role in coastal erosion and inundation when coupled with rising sea levels[4], as well as their potential for renewable energy generation[5]. Although tropical cyclones can have some influence on the occurrence of large waves in subtropical regions, the largest waves along the central east coast of Australia are most commonly attributable to extratropical cyclones[6]. The large waves caused by these storms can have severe impacts on coastal regions, such as being a major contributor to elevated water levels due to wave set-up[7]. Large waves can also have desirable benefits for coastal areas including recreational pursuits such as surfing, as well as influencing biodiversity within ocean ecosystems[8]. Any projected change in the future wave height spectrum could therefore be expected to have both desirable and undesirable impacts on coastal regions.

The diagnostic method used here to produce projections of large wave occurrence is based on geopotential height in the upper troposphere. Previous studies have examined contour maps of geopotential height for eastern Australia, finding that a strong curvature of the contours provides a good indication of the likelihood of extratropical cyclone occurrence[9–11]. To examine whether or not this is also the case for large wave occurrence, Figure 1 shows contour maps of geopotential height (at the 500 hPa pressure level obtained from the European Centre for Medium-Range Weather Forecasts ERA-Interim reanalyses[12]) for four different wave height ranges: 6 m or larger, 4–6 m, 2–4 m and 2 m or smaller. Wave height is calculated as the largest wave height observed on a given day at any one of five ocean buoys[13] along the central east coast of Australia. The contour maps represent the average of all days when the wave height was within the specified range, calculated for the period of available wave observations (from 1992 to 2010).

For wave heights of 6 m or larger (Fig. 1a), a strong curvature is apparent in the contour map of geopotential height over eastern Australia. There is some curvature in the contour map for waves in the height range 4–6 m (Fig. 1b), although this curvature is not as strong as for the largest wave height range (Fig. 1a). There is very little curvature of the contours for the two smaller wave height ranges (Fig. 1c,d). This shows that the curvature of the geopotential height contours can be used to provide an indication of the risk of large wave occurrence in this region.

To quantify the curvature of the geopotential height field, a daily time series is produced for the period from 1992 to 2010 of the maximum geostrophic vorticity from any location within the diagnostic region (shown as the black rectangles in Fig. 1). The 10% of days in this time series that have the strongest cyclonic vorticity are defined as diagnostic event days. This value of 10% is chosen to match the occurrence frequency of storms in this region[14]. Figure 2 shows the distribution of the largest wave height recorded from any one of the five buoys on a given day, as well as the number of diagnostic event days (based on ERA-Interim reanalyses[12]) that occurred for each wave height range. Diagnostic event days correspond to a higher proportion of days towards the upper tail of the wave height distribution than towards the lower tail of the distribution. This is not the case for days on which tropical cyclones occurred near eastern Australia (shown in Fig. 2 as red triangles, based on tropical cyclone observations in the South Pacific region from 150° E to 180° (refs 15,16)), consistent with the results of previous studies showing that extratropical cyclones are the dominant cause of large waves in this region[6].

The diagnostic method is applied here to examine projections of the future wave climate based on 18 different GCMs from the Coupled Model Intercomparison Project Phase 5 (CMIP5; ref. 17) set of GCMs. Figure 3 shows the annual number of diagnostic event days for each of the 18 GCMs, with a 30-year smoothing applied to show the climate signal (that is, a 30-year moving average). Diagnostic event days are defined for the historical time period (from 1950 to 2005) as the 10% of days that have the strongest cyclonic geostrophic vorticity. This is done individually for each GCM, such that each GCM has a unique threshold

Centre for Australian Weather and Climate Research, Bureau of Meteorology, 700 Collins St, Docklands, Victoria 3008, Australia.
*e-mail: a.dowdy@bom.gov.au

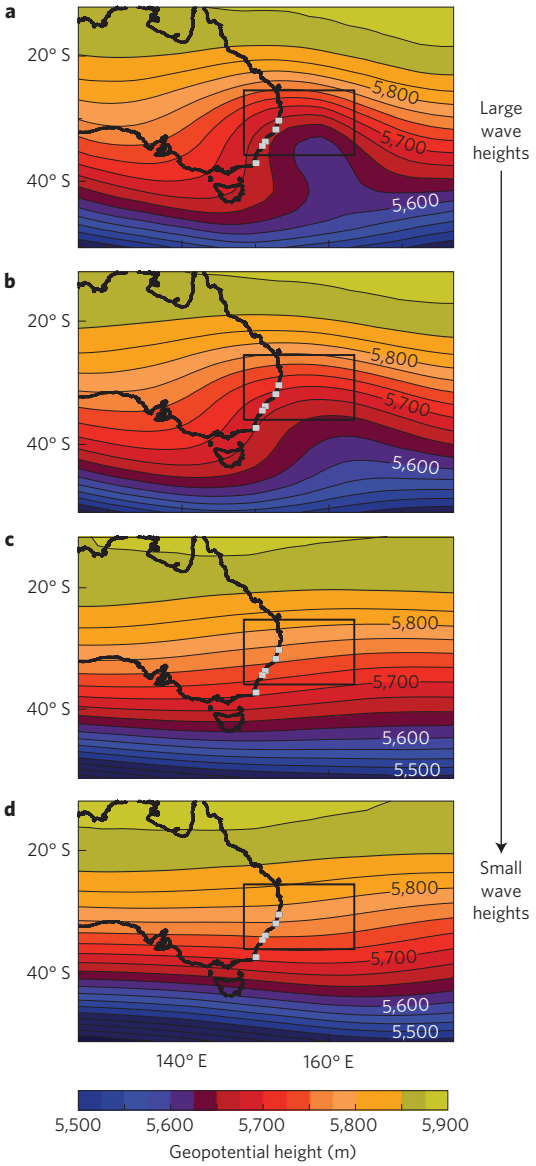

Figure 1 | Contour maps of geopotential height over eastern Australia for different wave height ranges. The contour maps represent the average for all days with wave heights in the following ranges: **a**, 6 m or larger; **b**, 4–6 m; **c**, 2–4 m; and **d**, 2 m or smaller. Wave height is calculated as the largest value recorded from any one of five offshore buoys (grey squares) on a given day during the period 1992–2010. The Australian coastline is shown, as is the region used to calculate the diagnostic (black rectangle).

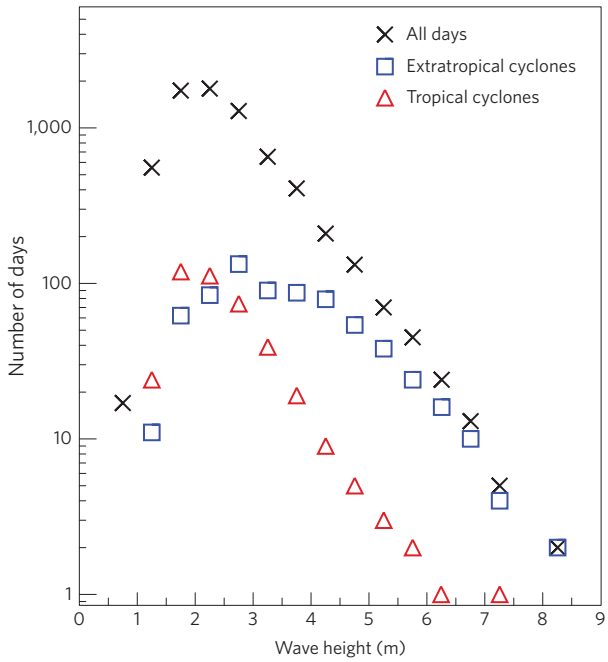

Figure 2 | Wave heights from ocean buoy observations during the period 1992–2010, distributed in 0.5 m height ranges. Wave height distributions are shown for all days (black crosses), as well as for days on which extratropical cyclones occurred as indicated by diagnostic event days (blue squares) and for days on which tropical cyclones occurred in the South Pacific region from 150° E to 180° (red triangles).

value of geostrophic vorticity for defining a diagnostic event day (as listed in Supplementary Table 2). The threshold value for the historical time period is subsequently applied to examine how many diagnostic event days occur in the future climate projections (from 2006 to 2100). Two different emission pathways are examined: an intermediate-emission pathway (representative concentration pathway 4.5, RCP4.5, with atmospheric greenhouse gas concentrations stabilized this century) and a relatively high-emission pathway (RCP8.5, with no stabilization this century)[18].

The annual number of diagnostic event days reduces from 36 during the historical period to 27 for the intermediate-emission pathway and to 21 for the high-emission pathway (based on the mean for the time period from 2070 to 2100). These changes are more than three times larger in magnitude than the level of uncertainty shown by the standard error of the mean in Fig. 3, thereby indicating a clear reduction in the frequency of occurrence of diagnostic event days towards the end of the twenty-first century.

The annual number of diagnostic event days based on ERA-Interim reanalyses shows some indication of a decreasing trend (Fig. 3 and Supplementary Fig. 3), while noting that the GCM simulations of the historical and future climate allow this trend to be examined over a much longer time period than the 32-year period of reanalyses. The values based on reanalyses in Fig. 3 have a five-year moving average applied and therefore show more short-term variability than the GCM values that have a 30-year moving average applied to show the climate signal.

A change in the frequency of occurrence of diagnostic event days can be expected to have a varying effect on different parts of the wave height distribution. This is owing to the fact that diagnostic event days correspond to an increasing proportion of the wave height distribution for increasing wave heights, ranging from 0% of the days with the smallest wave heights up to 100% of the days with the largest wave heights (from Fig. 2). Projected changes in the wave height distribution are shown in Table 1 (based on applying equation (1), Methods) and are predominantly characterized by a reduction in the upper tail of the distribution with a relatively small increase in the lower tail. This is the case for both emission pathways, with larger magnitude changes for high emissions (RCP8.5) than for intermediate emissions (RCP4.5).

Statistical downscaling studies of the wave climate are typically based on mean sea level pressure (MSLP) fields[2,3,19,20]: the diagnostic method used here is very new in that it is not based on surface fields, thereby providing a somewhat independent perspective from previous studies. Independence between study methods is a desirable quality, given that variance between different study methods is a dominant source of uncertainty in wave projections[21]. The storm wave projections presented here are broadly consistent with a wide variety of different studies. For example, a significant decreasing trend in storminess has been observed based on

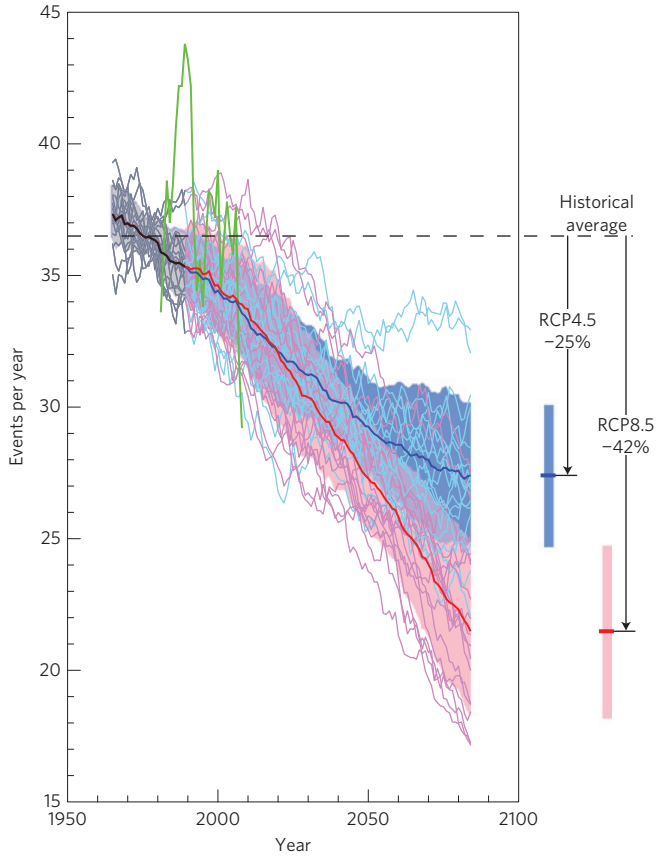

Figure 3 | Annual number of large wave days as indicated by the diagnostic. Projections from 18 GCMs are shown for intermediate (blue, RCP4.5) and high (red, RCP8.5) greenhouse gas emission pathways, as well as for the historical period (black). A 30-year moving average is applied to show the climate signal. The mean values of the 18 GCMs are shown (thick lines), as well as the standard error of the mean (shaded regions: representing one standard error above and below the mean). The mean and standard error for the period 2070–2100 are shown for RCP4.5 and RCP8.5 (coloured bars on the right of the figure) for comparison with the historical average number of events (dashed black line). Values based on ERA-Interim reanalyses are shown (green) with a five-year moving average applied for the period 1979–2010.

instrument records of MSLP in southeast Australia from 1885 to 2008[22]. A statistical downscaling study based on MSLP fields from one GCM in the CMIP3[23] database projected a reduction in large wave occurrence for eastern Australia during winter[3], noting that most large waves events occur during winter along Australia's central east coast. A future reduction in large waves was projected to occur for this region[24] based on dynamical downscaling from three different CMIP3 GCMs. Wind projections also indicate a future reduction in the 99th percentile wind speeds near the central east coast of Australia[25]. Although these methods each have various different uncertainties associated with them, the similarity of the results derived from these contrasting methods provides a considerable degree of confidence in the projections of fewer large wave events in this region, as does the high degree of consistency in results between the 18 different CMIP5 GCMs presented here.

The high level of consistency between different GCMs for the projections presented here suggests that the use of a large-scale upper-tropospheric diagnostic suits the strengths and scales of current GCMs, noting that the useful size of a geographic domain for representing storm occurrence tends to increase with height in the troposphere (for example, storm size is typically larger at 500 hPa than at the surface[26,27]). The projections presented here are likely to be related to projected changes in a number of different large-scale phenomena, including Rossby wave activity[28] and a split in the subtropical jet stream over eastern Australia during winter[29], given that the diagnostic method is sensitive to the strong upper-tropospheric vorticity that characterizes these phenomena.

Table 1 | Projected changes in the wave height distribution.

Wave height (m)	Intermediate emissions (%)	High emissions (%)
0–2	+2	+3
2–4	0	0
4–6	−9	−15
>6	−16	−28

The projections are for the end of the twenty-first century (that is, the average for the time period from 2070 to 2100), calculated as the percentage change from the historical time period (from 1950 to 2005) in the frequency of occurrence of waves within a given height range. The projected changes are shown in 2 m height intervals, for intermediate (RCP4.5) and high (RCP8.5) emission pathways.

The difference between the intermediate- and high-emission pathways in Fig. 3 is equal to six diagnostic event days per year on average during the 2070–2100 time period. This is about twice as large as the standard error of the mean during this period (equal to 2.6 and 3.2 events per year for RCP4.5 and RCP8.5 emission pathways, respectively), allowing the importance of the magnitude of the emissions to be clearly demonstrated. This is different from previous studies that have reported differences between models that are considerably larger than differences between emission scenarios[2].

An increased understanding of the future wave climate will lead to improved planning and preparedness for changes in the impacts (both desirable and undesirable) of large wave events on the coastal zone. Although this study projects a future reduction in the occurrence frequency of large waves associated with storminess in this region, it is possible that the storms that do occur could become more intense[29]. Furthermore, the effects of rising sea levels will act to increase the impacts associated with large wave events on coastal regions, including erosion and inundation, highlighting the complexities associated with adapting to climatological changes in the upper tail of the wave height spectrum.

Methods

For a detailed description of the methods see Supplementary Methods.

Wave observations. Wave height data were obtained from a series of buoys[13] located about 6–12 km off the coast in deep water (~70 m). The buoys use an accelerometer to measure changes in vertical motion as they move with the water surface. Daily significant wave height data are used here, representing the mean wave height of the highest third of the wave data. Data were available for use in this study during the time period 1992–2010 from five buoys located between 30° S and 38° S (Fig. 1 and Supplementary Fig. 1, Table 1).

Tropical cyclone observations. Tropical cyclone observations were obtained from a data set created and maintained by the National Climate Centre of the Australian Bureau of Meteorology, as described in previous studies[15,16]. The wave height distribution for days on which tropical cyclones occurred (Fig. 2) is based on tropical cyclone observations in the South Pacific region from 150° E to 180°.

Description of the diagnostic method. The diagnostic method is based on 500 hPa geostrophic vorticity calculated as the Laplacian of geopotential divided by the Coriolis parameter[10]. First, geostrophic vorticity at a given time is calculated at every individual location (using gridded data) within a geographic region of 15° in longitude and 10.5° in latitude (shown as the black rectangles in Fig. 1). Second, a daily time series is produced of the maximum magnitude of cyclonic (that is, negative in the Southern Hemisphere) geostrophic vorticity within this geographic region. Third, the 90th percentile of this daily time series is calculated. Fourth, days on which the time series exceeds its 90th percentile are defined as diagnostic event days. Diagnostic event days therefore represent the

10% of days with the strongest cyclonic geostrophic vorticity at any location within the diagnostic region. Previous studies have detailed the application of the diagnostic method to a variety of different reanalyses and GCMs[10,11].

Application to reanalyses. The diagnostic method is applied here to ERA-Interim reanalyses[12] with 1.5 degree resolution in both latitude and longitude and six-hourly temporal resolution. A one-day running mean is applied to the six-hourly data to reduce small-scale temporal variability. The diagnostic is produced here using a time lag of 6 h with respect to the timing of the wave observations, as this produces the best diagnostic skill (Supplementary Fig. 2).

Application to GCMs. The application of the diagnostic to GCMs requires spatial fields of 500 hPa geopotential height with daily (or shorter) temporal resolution. In conjunction with the Intergovernmental Panel on Climate Change, a set of GCM experiments has been produced: the World Climate Research Program CMIP5[17]. Of the more than 50 models in the CMIP5 data set, 22 had archived daily 500 hPa geopotential height fields. Four of these 22 models were not consistent with the requirements of the study method (for reasons detailed in Supplementary Information), such that 18 GCMs were available for use in this study (as listed in Supplementary Table 2).

The diagnostic method is applied to the 18 GCMs to examine projected changes in the frequency of occurrence of diagnostic event days. A change in the frequency of occurrence of diagnostic event days will also produce a change of equal magnitude and opposite sign in the occurrence frequency of non-diagnostic event days, so as to conserve the total number of days. This condition is described by equation (1), based on applying a projected change of X% (that is, −25% for RCP4.5 and −42% for RCP8.5) over the historical distribution of diagnostic event days (as shown in Fig. 2) and applying a change of $-X/9$% over the historical distribution of non-diagnostic event days (noting that there are nine times more non-diagnostic event days than diagnostic event days during the historical period).

$$W_{\mathrm{proj}}(h) - W_{\mathrm{hist}}(h) = D_{\mathrm{hist}}(h) \times X - [W_{\mathrm{hist}}(h) - D_{\mathrm{hist}}(h)] \times \frac{X}{9} \qquad (1)$$

where h is wave height, $W_{\mathrm{proj}}(h)$ is the projected wave height distribution, $W_{\mathrm{hist}}(h)$ is the historical wave height distribution, $D_{\mathrm{hist}}(h)$ is the historical wave height distribution for diagnostic event days and X is the projected change in the number of diagnostic event days, noting that $[W_{\mathrm{hist}}(h) - D_{\mathrm{hist}}(h)]$ represents the historical wave height distribution for non-diagnostic event days.

Received 18 July 2013; accepted 24 January 2013; published online 9 March 2014

References

1. Hemer, M. A., McInnes, K. L. & Ranasinghe, R. Climate and variability bias adjustment of climate model-derived winds for a southeast Australian dynamical wave model. *Ocean Dynam.* **62,** 87–104 (2012).
2. Wang, X. L. & Swail, V. R. Climate change signal and uncertainty in projections of ocean wave heights. *Clim. Dynam.* **26,** 109–126 (2006).
3. Caires, S., Swail, V. R. & Wang, X. L. Projection and analysis of extreme wave climate. *J. Clim.* **19,** 5581–5605 (2006).
4. Webb, E. L. *et al.* A global standard for monitoring coastal wetland vulnerability to accelerated sea-level rise. *Nature Clim. Change* **3,** 458–465 (2013).
5. Hemer, M. A. & Griffin, D. A. The wave energy resource along Australia's southern margin. *J. Renew. Sust. Energy* **2,** 043108 (2010).
6. Short, A. D. & Trenaman, N. L. Wave climate of the Sydney region, an energetic and highly variable ocean wave regime. *Aust. J. Mar. Freshwat. Res.* **43,** 765–791 (1992).
7. McInnes, K. L., Hubbert, G. D., Abbs, D. J. & Oliver, S. E. A numerical modelling study of coastal flooding. *Met. Atmos. Phys.* **80,** 217–233 (2002).
8. England, P. R., Phillips, J., Waring, J. R., Symonds, G. & Babcock, R. Modelling wave-induced disturbance in highly biodiverse marine macroalgal communities: Support for the intermediate disturbance hypothesis. *Mar. Freshwat. Res.* **59,** 515–520 (2008).
9. Mills, G. A. *et al. Centre for Australian Weather and Climate Research, Australia, CAWCR* Technical Report 23 (Australian Weather and Climate Research, 2010).
10. Dowdy, A. J., Mills, G. A. & Timbal, B. Large-scale diagnostics of extratropical cyclogenesis in eastern Australia. *Int. J. Climatol.* **33,** 2318–2327 (2013).
11. Dowdy, A. J., Mills, G. A., Timbal, B. & Wang, Y. Changes in the risk of extratropical cyclones in eastern Australia. *J. Clim.* **26,** 1403–1417 (2013).
12. Dee, D. P. *et al.* The ERA-Interim reanalysis: Configuration and performance of the data assimilation system. *Q. J. R. Meteorol. Soc.* **137,** 553–597 (2011).
13. Kulmar, M., Lord, D. & Sanderson, B. in *Coasts and Ports: Coastal Living—Living Coast; Australasian Conference 2005; Proceedings* (eds Townsend, M. R. & Walker, D.) 167–172 (Institution of Engineers, 2005).
14. Speer, M. S., Wiles, P. & Pepler, A. Low pressure systems off the New South Wales coast and associated hazardous weather: Establishment of a database. *Aust. Meteorol. Oceanogr. J.* **58,** 29–39 (2009).
15. Dowdy, A. J. *et al.* Tropical cyclone climatology of the South Pacific Ocean and its relationship to the El Niño-Southern Oscillation. *J. Clim.* **25,** 6108–6122 (2012).
16. Dowdy, A. J. & Kuleshov, Y. An analysis of tropical cyclone occurrence in the Southern Hemisphere derived from a new satellite-era dataset. *Int. J. Remote Sens.* **23,** 7382–7397 (2012).
17. Taylor, K. E., Stouffer, R. J. & Meehl, G. A. An overview of CMIP5 and the experiment design. *Bull. Am. Meteorol. Soc.* **93,** 485–498 (2012).
18. Van Vuuren, D. P. *et al.* RCP2.6: Exploring the possibility to keep global mean temperature change below 2 degrees. *Climatic Change* **109,** 5–31 (2011).
19. Izaguirre, C. *et al.* Exploring the interannual variability of extreme wave climate in the northeast Atlantic Ocean. *Ocean Model.* **59–60,** 31–40 (2012).
20. Wang, X. L., Feng, Y. & Swail, V. R. North Atlantic wave height trends as reconstructed from the 20th century reanalysis. *Geophys. Res. Lett.* **39,** L18075 (2012).
21. Hemer, M. A., Fan, Y., Mori, N., Semedo, A. & Wang, X. L. Projected changes in wave climate from a multi-model ensemble. *Nature Clim. Change* **3,** 471–476 (2013).
22. Alexander, L., Wang, X., Wan, H. & Trewin, B. Significant decline in storminess over south-east Australia since the late 19th century. *Aust. Meteorol. Oceanogr. J.* **61,** 23–30 (2011).
23. Meehl, G. *et al.* The WCRP CMIP3 multi-model dataset: A new era in climate change research. *Bull. Am. Meteorol. Soc.* **88,** 1383–1394 (2007).
24. Hemer, M. A., McInnes, K. L. & Ranasinghe, R. Projections of climate change-driven variations in the offshore wave climate off south eastern Australia. *Int. J. Climatol.* **33,** 1615–1632 (2012).
25. McInnes, K. L., Erwin, T. A. & Bathols, J. M. Global climate model projected changes in 10 m wind speed and direction due to anthropogenic climate change. *Atmos. Sci. Lett.* **12,** 325–333 (2011).
26. Campins, J., Jansà, A. & Genovés, A. Three-dimensional structure of western Mediterranean cyclones. *Int. J. Climatol.* **26,** 323–343 (2006).
27. Lim, E-P. & Simmonds, I. Southern Hemisphere winter extratropical cyclone characteristics and vertical organization observed with the ERA-40 data in 1979–2001. *J. Clim.* **20,** 2675–2690 (2007).
28. Freitas, A. C. V. & Rao, V. B. Global changes in propagation of stationary waves in a warming scenario. *Q. J. R. Meteorol. Soc.* http://dx.doi.org/10.1002/qj.2151 (2013).
29. Grose, M. R., Pook, M. J., McIntosh, P. C., Risbey, J. S. & Bindoff, N. L. The simulation of cutoff lows in a regional climate model: Reliability and future trends. *Clim. Dynam.* **39,** 445–459 (2012).

Acknowledgements

This study was financially supported by the Australian Climate Change Science Program (ACCSP) project grant, The Influence of Climate Change on East Coast Lows. The authors would like to thank M. Hemer from CSIRO and R. Colman from the Australian Bureau of Meteorology for providing comments on an initial draft of this manuscript.

Author contributions

A.J.D. conceived the study and wrote the paper. Analysis was carried out by A.J.D. and Y.W. The manuscript was discussed and revised by all authors. All figures were produced by A.J.D., except Fig. 3 produced by A.J.D. and Y.W.

Additional information

Supplementary information is available in the online version of the paper. Reprints and permissions information is available online at www.nature.com/reprints. Correspondence and requests for materials should be addressed to A.J.D.

Competing financial interests

The authors declare no competing financial interests.